

Control of crystalline phase and morphology of calcium carbonate by electrolysis: Effects of current and temperature

著者	Miyazaki Toshiki, Arie Takashi, Shirotsuki Yuki
journal or publication title	Ceramics International
volume	45
number	11
page range	14039-14044
year	2019-04-19
URL	http://hdl.handle.net/10228/00008196

doi: <https://doi.org/10.1016/j.ceramint.2019.04.103>

Manuscript Number: CERI-D-18-09086R1

Title: Control of crystalline phase and morphology of calcium carbonate by electrolysis: effects of current and temperature

Article Type: Full length article

Keywords: Powders: chemical preparation; Biomedical applications; CaCO₃

Corresponding Author: Dr. Toshiki Miyazaki,

Corresponding Author's Institution: Kyutech

First Author: Toshiki Miyazaki

Order of Authors: Toshiki Miyazaki; Takashi Aii; Yuki Shiroaki

Abstract: Calcium carbonate (CaCO₃) can show various properties related to its different crystalline phases. For example, the aragonite phase has excellent mechanical strength, whereas the vaterite phase has high water solubility. Therefore, CaCO₃ is a useful material for various applications. Wet processes are known to be suitable for preparing metastable CaCO₃ polymorphs. Electrolysis has been proposed as a preparation method at ambient conditions. Although several electrolytic approaches have been reported, the effects of the applied current and temperature of the electrolyte on the crystalline phase and morphology of CaCO₃ remain unclear. In the present study, we attempted the electrochemical preparation of CaCO₃ particles with various electrolysis conditions and discuss the mechanism of CaCO₃ particle formation. The crystalline phase and morphology of the CaCO₃ precipitates markedly changed depending on the applied current and method of cooling the electrolyte. We assume that these factors were governed by the degree of change in temperature, supersaturation and pH of the electrolyte induced by differences in the electrolysis current.

1
2
3 **Control of crystalline phase and morphology of calcium carbonate by**
4 **electrolysis: effects of current and temperature**
5
6

7 Toshiki Miyazaki^a, Takashi Arii^a and Yuki Shirosaki^b
8
9

10
11 ^aGraduate School of Life Science and System Engineering, Kyushu Institute of
12 Technology, Kitakyushu, Japan
13
14

15
16 ^bFaculty of Engineering, Kyushu Institute of Technology, Kitakyushu, Japan
17
18
19
20
21

22 Corresponding author:
23

24 Toshiki Miyazaki
25

26
27 Graduate School of Life Science and Systems Engineering, Kyushu Institute of
28 Technology, 2-4, Hibikino, Wakamatsu-ku, Kitakyushu 808-0196, Japan
29
30

31 Tel/Fax: +81-93-695-6025
32

33 E-mail: tmiya@life.kyutech.ac.jp
34
35
36
37
38
39
40
41
42
43
44
45
46
47
48
49
50
51
52
53
54
55
56
57
58
59
60
61
62
63
64
65

1
2
3 **Abstract**
4
5
6

7 Calcium carbonate (CaCO_3) can show various properties related to its different
8
9
10 crystalline phases and is therefore a useful material for various applications. Wet
11
12
13 processes are known to be suitable for preparing metastable CaCO_3 polymorphs.
14
15
16 Electrolysis has been proposed as a preparation method at ambient conditions. Although
17
18
19 several electrolytic approaches have been reported, the effects of the applied current and
20
21
22 temperature of the electrolyte on the crystalline phase and morphology of CaCO_3 remain
23
24
25 unclear. In the present study, we attempted the electrochemical preparation of CaCO_3
26
27
28 particles under various electrolysis conditions and discuss the mechanism of CaCO_3
29
30
31 particle formation. The crystalline phases and morphologies of the CaCO_3 precipitates
32
33
34 markedly changed depending on the applied current and method of cooling the
35
36
37 electrolyte. We assume that these factors were governed by the degree of change in
38
39
40 temperature, supersaturation, and pH of the electrolyte that were induced by differences
41
42
43 in the electrolysis current.
44
45
46
47
48
49
50

51 **Keywords:** A: Powders: chemical preparation, E: Biomedical applications, CaCO_3
52
53
54
55
56
57
58
59
60
61
62
63
64
65

1
2
3 **Introduction**
4
5
6

7 Calcium carbonate (CaCO_3), an inorganic substance composed of common elements,
8
9
10 has attracted considerable attention as a material with a low environmental burden and
11
12
13 low risk of resource depletion. CaCO_3 exhibits various properties that depend on its
14
15
16 crystalline phase; for example, the aragonite phase has excellent mechanical strength
17
18
19 owing to its high density [1], whereas the vaterite phase has high water solubility [2]. In
20
21
22 the field of biomaterials, vaterite has attracted attention as a novel bioresorbable
23
24
25 material with high biological affinity. A nonwoven fabric for bone repair has been
26
27
28 prepared from vaterite and poly-L-lactic acid by electrospinning [3] and bioresorbable
29
30
31 vaterite microspheres combined with silicate have been developed for bone-forming
32
33
34 applications [4].
35
36
37
38
39
40
41

42 Wet processes are suitable for preparing CaCO_3 with a metastable phase. Crystalline
43
44
45 phase control has been attempted by addition of organic substances in aqueous
46
47
48 precipitation processes [5,6]. Furthermore, electrolysis has been proposed as a method
49
50
51 to prepare CaCO_3 polymorphs at ambient conditions. Watanabe et al. applied an
52
53
54 alternating current of 10 V/cm to a glass cell containing calcium chloride and sodium
55
56
57
58
59
60
61
62
63
64
65

1
2
3 carbonate solutions separated by a membrane and obtained a mixture of calcite and
4
5
6
7 vaterite with a small amount of aragonite [7]. Yamada et al. applied a direct current of 3
8
9
10 to 10 V to a cell containing calcium nitrate and sodium hydrogen carbonate (NaHCO₃)
11
12
13 solutions separated by a membrane. In this case, addition of sodium nitrate to the
14
15
16
17 electrolyte effectively enhanced the formation of both calcite and vaterite [8]. The
18
19
20 effects of the electrolysis conditions on the crystalline phase and morphology of CaCO₃
21
22
23
24 nevertheless remain unclear.
25
26

27
28 In the present study, we attempted to prepare CaCO₃ particles by an electrochemical
29
30
31 method by varying the direct electric current and temperature. We discuss the
32
33
34
35 mechanism of CaCO₃ formation in detail.
36
37
38
39
40
41

42 **Materials and Methods**

43
44
45 Calcium nitrate tetrahydrate [Ca(NO₃)₂·4H₂O] and hydrochloric acid (HCl) were
46
47
48 purchased from Wako Pure Chemical Co., Japan. NaHCO₃ and
49
50
51
52 tris(hydroxymethyl)aminomethane (Tris) were purchased from Nacalai Tesque Inc.,
53
54
55
56 Japan. The electrolytic cell is shown in Figure 1. The anode and cathode chambers were
57
58
59
60
61

1
2
3 filled with 100 mL of 0.5 M $\text{Ca}(\text{NO}_3)_2$ aqueous solution and an equal volume of 0.5 M
4
5
6
7 NaHCO_3 aqueous solution, respectively. Both solutions were buffered at pH 8.5 by Tris
8
9
10 and HCl. The reaction compartment between the chambers was filled with 220 mL of
11
12
13 Tris buffer at pH 8.5. Platinum foils (Nilaco Co., Japan), 50 mm \times 10 mm \times 0.1 mm in
14
15
16 size, were used for the electrodes. Constant direct current (DC) ranging from 0.2 to 0.6
17
18
19 A was applied by a power supply (ZX-400M, Takasago Ltd., Japan) to the cell for
20
21
22 various periods up to 30 min. At some conditions, the temperature of the electrolyte in
23
24
25 the cell was controlled by use of cooling water and ice. Precipitates that formed in the
26
27
28 reaction chamber were collected by vacuum filtration and dried at 60 °C.
29
30
31
32
33

34
35 The microstructure of the precipitates was analyzed by powder X-ray diffraction
36
37
38 (XRD; MXP3V, Mac Science Co., Japan) with a $\text{CuK}\alpha$ X-ray source operating at 40 kV
39
40
41 and 30 mA. We also performed scanning electron microscope (SEM; S-3500N, Hitachi
42
43
44 Co., Japan) and transmission electron microscope (TEM; H-9000NAR, Hitachi Co.,
45
46
47 Japan) imaging studies. For SEM observations, the sample surface was coated with
48
49
50 Au–Pd alloy by ion sputtering (E-101, Hitachi Co., Japan). A focused ion beam (FIB,
51
52
53 FB-2000A, Hitachi Co., Japan) was used to prepare thin films for TEM observations.
54
55
56
57
58
59
60
61
62
63
64
65

1
2
3
4
5
6
7 **Results**
8

9
10 For all conditions, white precipitates were observed in the reaction chamber about 2
11 min after applying the DC electric field. XRD patterns of precipitates obtained at
12 various currents without temperature control or with ice cooling are shown in Figure 2.
13
14
15
16
17
18
19
20

21 At 0.2 and 0.4 A without temperature control, calcite, vaterite, and a small amount of
22 aragonite were formed; the amount of calcite was greater than that of the other phases.
23
24
25
26
27

28 Conversely, vaterite was the main crystalline phase and a small amount of calcite was
29 formed at 0.4 A with ice cooling. In addition, the amount of aragonite formed at 0.6 A
30 was much greater than in any of the other samples.
31
32
33
34
35
36
37

38 SEM images of the precipitates obtained at various currents without temperature
39 control or with ice cooling are shown in Figure 3. The morphologies of the precipitates
40 changed markedly depending on the current value and cooling method, as summarized
41 in Table 1. The shapes of the particles, as shown in Table 1, are schematically illustrated
42 in Fig. 4.
43
44
45
46
47
48
49
50
51
52
53

54
55
56 The temperature increased as the current was increased (Figure 5). Even with
57
58
59
60
61
62
63
64
65

1
2
3 ice cooling, at 0.4 A, the temperature increased to 45 °C within 30 min. We assume that
4
5
6
7 the heat generated by the electrolyte at 0.4 A was too high to be maintained at a constant
8
9
10 temperature by the ice bath.
11

12
13 Figure 6 shows XRD patterns of precipitates obtained at constant temperature and 0.2
14
15
16
17 A. The peak intensity of the vaterite increased as the temperature increased and the
18
19
20 amount of calcite formed was slightly higher at 30 °C than at other temperatures.
21
22
23

24 Figure 7 shows SEM images of precipitates obtained at constant temperature and 0.2
25
26
27
28 A. The morphology of the vaterite particles changed from spherical to
29
30
31 hexagonal-shaped, and finally to flower-like, as the temperature was increased (Table
32
33
34
35 1).
36
37

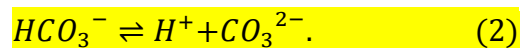
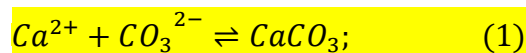
38 SEM images of the spherical particles prepared at 0.2 A and 25 °C are shown in
39
40
41
42 Figure 8 at low and high magnification. Spherical vaterite was covered with many
43
44
45 nanoparticles, of 50 to 100 nm in size.
46
47

48 TEM images and electron diffraction patterns of the surface and inside of particles
49
50
51 prepared at 0.4 A with ice cooling are shown in Figure 9. Diffraction rings and
52
53
54
55
56 diffraction spots from the (200) spacing of vaterite were observed on the surface and
57
58
59
60
61

1
2
3 inside of the particles, respectively; thus, the surface and inside of the hexagonal
4
5
6
7 particles comprised vaterite polycrystals and single crystals with c-axis orientation,
8
9
10 respectively.
11

12 13 14 15 16 17 **Discussion** 18

19
20 CaCO_3 was precipitated by simple electrolysis reactions. Ca^{2+} diffuses from the
21
22
23
24 anode to the cathode under a DC electric field, while CO_3^{2-} diffuses in the reverse
25
26
27
28 direction. Limiting ionic conductance of Ca^{2+} ($119.0 \text{ S}\cdot\text{cm}^2/\text{mol}$) is relatively close to
29
30
31 that of CO_3^{2-} ($138.6 \text{ S}\cdot\text{cm}^2/\text{mol}$) [9], which means that their ionic mobilities are also
32
33
34
35 similar; therefore, precipitation of CaCO_3 would not occur in the anode or cathode
36
37
38
39 chamber, but in the reaction chamber. It is known that about 95 mol% of carbonate ion
40
41
42 exists in the form of HCO_3^- at pH 8.5 [10]. CaCO_3 with low water solubility is formed
43
44
45 by Equation (1) to consume CO_3^{2-} ; therefore, the equilibrium in Equation (2) is shifted
46
47
48
49 to the right:
50



1
2
3 We found that the crystalline phase of electrochemically produced CaCO_3 can be
4
5
6 controlled by the applied current. The aragonite phase, which is normally difficult to
7
8
9 obtain by electrolytic methods, was obtained by increasing the current. Generally,
10
11
12 aragonite can be prepared in solutions at high temperatures [11]; therefore, increasing
13
14
15 the electrolyte temperature at high current promoted aragonite formation. Monolithic
16
17
18 aragonite was not obtained in the present study. Wang et al. demonstrated that
19
20
21 monolithic aragonite is difficult to obtain without stirring of the solution, even at high
22
23
24 temperature [12]. Monolithic samples are preferable for many practical applications;
25
26
27 therefore, the addition of flow apparatus to our reaction chamber or addition of an
28
29
30 aragonite stabilizer, such as Mg^{2+} , might be applied to our system to achieve such
31
32
33 morphology.
34
35
36
37
38
39
40
41

42 The crystalline phases and morphologies of the precipitates was markedly affected by
43
44
45 the method of temperature control, even at the same current (see Figs. 2 and 3), i.e.,
46
47
48 particles with a hexagonal shape formed at 0.4 A with ice cooling, whereas many
49
50
51 flower-like particles formed under all current conditions without temperature control.
52
53
54

55
56 Kojima et al. prepared CaCO_3 particles with different crystalline phases and
57
58
59
60
61
62
63
64
65

1
2
3 morphologies by heating of $\text{Ca}(\text{HCO}_3)_2$ solutions at different temperatures and pH, and
4
5
6
7 precisely investigated the mechanism of CaCO_3 formation [13]. They showed that the
8
9
10 morphology of the vaterite changed from hexagonal to flower-like as the pH decreased.
11
12
13 In the present study, the pH of the electrolyte tended to decrease when temperature was
14
15
16 uncontrolled (i.e., pH 8.4 at 0.2 A and 30 °C after 30 min, compared with pH 7.9 at 0.2
17
18
19 A without temperature control), in agreement with the above study. Therefore,
20
21
22 decreasing pH promotes the formation of flower-like particles.
23
24
25
26
27

28 When the temperature of the electrolyte was maintained constant, the morphology of
29
30
31 the vaterite changed from hexagonal to flower-like as the temperature was increased
32
33
34 (see Fig. 7). The solubility of CaCO_3 decreases as temperature increases [14]; therefore,
35
36
37
38 an increase in the degree of supersaturation with respect to CaCO_3 at high temperature
39
40
41 promoted the formation of flower-like particles. We note that the morphology of the
42
43
44 present particles was governed not only by pH, but also by the degree of
45
46
47 supersaturation.
48
49
50
51

52 A greater amount of calcite was formed without temperature control than with ice
53
54
55 cooling, even at the same current of 0.4 A (see Fig. 2). When the temperature was set to
56
57
58
59
60
61
62
63
64
65

1
2
3 0.2 A, the amount of calcite was slightly greater at 30 °C than at other temperatures (see
4
5
6
7 Fig. 6). Kojima et al. demonstrated that a single phase of calcite was formed at 30 °C
8
9
10 [13]; therefore, we assume that the electrolyte temperature was maintained at
11
12
13 approximately 30 °C for a longer time for the former than the latter, giving rise to a
14
15
16
17 greater amount of calcite.
18
19
20

21 Spherical and hexagonal vaterite were observed at low and high temperatures,
22
23
24 respectively (see Figs. 8 and 9). Their formation mechanism is schematically illustrated
25
26
27 in Fig. 10. At low temperatures, small nuclei formed: their growth was suppressed
28
29
30 owing to the low degree of supersaturation, but nucleation was enhanced by ion
31
32
33 diffusion from the anodic and cathodic chambers and the subsequent increase in the
34
35
36 degree of supersaturation. Small crystallites aggregated to form spherical particles, as
37
38
39 shown in Fig. 8. Conversely, at high temperatures, the formed nuclei vigorously grew
40
41
42 into hexagonal particles, owing to the degree of high supersaturation, and then
43
44
45
46 secondary nucleation occurred by ion diffusion from the chambers.
47
48
49
50

51
52
53 Vaterite single crystals with a similar morphology to that of our particles in Fig. 9
54
55
56 were reported by Zhan et al. [15]. They investigated the formation process of vaterite
57
58
59
60
61
62
63
64
65

1
2
3 prepared by heating of an aqueous mixture of calcium nitrate, gelatin, and urea at
4
5
6
7 100 °C. Hexagonal crystals covered with nanoparticles formed at 6 h, which
8
9
10 transformed to single crystals with clear facets after 1 day. They speculated that the high
11
12
13 concentration of gelatin (10 mass%) played an important role in oriented aggregation
14
15
16 growth. In the present study, the organic Tris concentration in the electrolyte was only
17
18
19
20
21 50 mM; therefore, it would have a small influence on the crystal growth. The formation
22
23
24 of CaCO₃ mesocrystals in a DC electric field has also been reported [16]; therefore,
25
26
27 oriented aggregation growth of vaterite in the present study would be induced by the
28
29
30
31 applied electric field.
32
33

34
35 We expect that vaterite particles with different morphologies will have applications as
36
37
38 bioresorbable drug delivery carriers with desirable release profiles, because the surface
39
40
41 area differs between single crystals and polycrystals.
42
43
44
45
46
47
48

49 **Conclusions**

50
51
52 It was found that CaCO₃ particles with different crystalline phases and morphologies
53
54
55
56 can be electrochemically fabricated by changing the applied direct current and
57
58
59
60
61
62
63
64
65

1
2
3 electrolyte temperature. In particular, the aragonite phase, which is normally difficult to
4
5
6 obtain by electrolytic methods, was observed at high current. Knowledge from the
7
8
9
10 present study can provide a fundamental approach to designing CaCO₃ with desired
11
12
13 mechanical and biological properties by electrochemical processing.
14
15
16
17
18
19
20

21 **Acknowledgment**

22
23
24 We thank Andrew Jackson, PhD, and Kathryn Sole, PhD, from Edanz Group
25
26
27
28 (www.edanzediting.com/ac) for editing drafts of this manuscript.
29
30
31
32
33
34

35 **References**

- 36
37
38
39 1. J. Sun, B. Bhushan, Hierarchical structure and mechanical properties of nacre: a
40
41
42 review, RSC Adv. 2 (2012) 7617-7632. <https://doi.org/10.1039/C2RA20218B>
43
44
45
46 2. L.N. Plummer, E. Busenberg, The solubilities of calcite, aragonite and vaterite in
47
48
49 CO₂-H₂O solutions between 0 and 90°C, Geochim. Cosmochim. Acta, 46 (1982)
50
51
52 1011-1040. [https://doi.org/10.1016/0016-7037\(82\)90056-4](https://doi.org/10.1016/0016-7037(82)90056-4)
53
54
55
56 3. A. Obata, T. Hotta, T. Wakita, Y. Ota, T. Kasuga, Electrospun microfiber meshes of
57
58
59
60
61
62
63
64
65

- 1
2
3 silicon-doped vaterite/poly (lactic acid) hybrid for guided bone regeneration, *Acta*
4
5
6
7 *Biomater.* 6 (2010) 1248-1257. <https://doi.org/10.1016/j.actbio.2009.11.013>
8
9
- 10 4. J. Nakamura, G. Poologasundarampillai, J.R. Jones, T. Kasuga, Tracking the
11
12 formation of vaterite particles containing aminopropyl-functionalized
13
14 silsesquioxane and their structure for bone regenerative medicine, *J. Mater. Chem.*
15
16
17
18 *B* 1 (2013) 4446-4454. <https://doi.org/10.1039/C3TB20589D>
19
20
21
22
- 23 5. N. Hosoda, T. Kato, Thin-film formation of calcium carbonate crystals: effects of
24
25 functional groups of matrix polymers, *Chem. Mater.* 13 (2001) 688-693.
26
27
28
29
30
31
32 <https://doi.org/10.1021/cm000817r>
33
34
- 35 6. Y. Zhao, Z. Chen, H. Wang, J. Wang, Crystallization control of CaCO₃ by ionic
36
37
38 liquids in aqueous solution, *Cryst Growth Des.* 9 (2009) 4984-4986.
39
40
41
42
43 <https://doi.org/10.1021/cg900771c>
44
45
- 46 7. J. Watanabe, M. Akashi, Formation of various polymorphs of calcium carbonate on
47
48
49 porous membrane by electrochemical approach, *J. Cryst. Growth* 311 (2009)
50
51
52
53 3697-3701. <https://doi.org/10.1016/j.jcrysgr.2009.06.016>
54
55
- 56 8. K. Yamada, M. Ohta, K. Hirano, T. Kimura, Preparation of calcium carbonate in an
57
58
59
60
61
62
63
64
65

1
2
3 electrolytic cell, *Inorg. Mater.*, 4 (1997) 609-612 (in Japanese).
4
5

6
7 9. J.A. Dean, *Lange's Handbook of Chemistry*, fifteenth ed., McGraw-Hill, New York,
8
9 1999.
10
11

12
13 10. K.M. Steel, K. Alizadehhesari, R.D. Balucan, B.Bašić, Conversion of CO₂ into
14
15 mineral carbonates using a regenerable buffer to control solution pH, *Fuel*, 111
16
17 (2013) 40-47. <https://doi.org/10.1016/j.fuel.2013.04.033>
18
19
20
21
22

23
24 11. Y. Ota, S. Inui, T. Iwashita, T. Kasuga, Y. Abe, Preparation conditions for aragonite
25
26 whiskers by carbonation process, *J. Ceram. Soc. Japan*, 104 (1996) 196-200 (in
27
28 Japanese). <https://doi.org/10.2109/jcersj.104.196>
29
30
31

32
33 12. H. Wang, W. Huang, Y. Han, Diffusion-reaction compromise the polymorphs of
34
35 precipitated calcium carbonate, *Particuology*, 11 (2013) 301-308.
36
37
38
39
40
41
42 <https://doi.org/10.1016/j.partic.2012.10.003>
43
44

45
46 13. Y. Kojima, A. Sadotomo, T. Yasue, Y. Arai, Control of crystal shape and
47
48 modification of calcium carbonate prepared by precipitation from calcium
49
50 hydrogencarbonate solution, *J. Ceram. Soc. Japan*, 100 (1992) 1145-1153 (in
51
52 Japanese). <https://doi.org/10.2109/jcersj.100.1145>
53
54
55
56
57
58

- 1
2
3
4 14. B. Coto, C. Martos, J.L. Peña, R. Rodríguez, G. Pastor, Effects in the solubility of
5
6
7 CaCO₃: experimental study and model description, Fluid Phase Equilibria, 324
8
9
10
11 (2012) 1-7. <https://doi.org/10.1016/j.fluid.2012.03.020>
12
13
14 15. J. Zhan, H.P. Lin, C.Y. Mou, Biomimetic formation of porous single-crystalline
15
16
17 CaCO₃ via nanocrystal aggregation, Adv. Mater., 15 (2003) 621-623.
18
19
20
21 <https://doi.org/10.1002/adma.200304600>
22
23
24
25 16. J. Qi, R. Guo, Y. Wang, X. Liu, H. Chan, Electric field-controlled crystallizing
26
27
28 CaCO₃ nanostructures from solution, Nanoscale Res. Lett. 11 (2016) 120.
29
30
31
32 <https://doi.org/10.1186/s11671-016-1338-4>
33
34
35
36
37
38
39
40
41
42
43
44
45
46
47
48
49
50
51
52
53
54
55
56
57
58
59
60
61
62
63
64
65

1
2
3 **Table caption**

4 **Table 1** Morphology of the precipitates prepared by various conditions
5
6

7
8 **Figure captions**

9 **Figure 1** Appearance of electrolytic cell.
10

11 **Figure 2** X-ray diffraction patterns of precipitates obtained at various currents without
12 temperature control and with ice cooling.
13

14 **Figure 3** Scanning electron micrograph of precipitates obtained at various currents
15 without temperature control and with ice cooling.
16

17 **Figure 4** Schematic illustration of shapes of precipitates formed under different
18 electrolytic conditions.
19

20 **Figure 5** Changes in temperature of the electrolyte.
21

22 **Figure 6** X-ray diffraction patterns of precipitates obtained at various constant
23 temperatures and 0.2 A.
24

25 **Figure 7** Scanning electron micrographs of precipitates obtained at various constant
26 temperatures and 0.2 A.
27

28 **Figure 8** Scanning electron micrographs of spherical particles prepared at 0.2 A and
29 25 °C at low and high magnifications.
30

31 **Figure 9** Transmission electron micrographs and electron diffraction patterns of the
32 surface and inside of particles prepared at 0.4 A with ice cooling.
33

34 **Figure 10** Schematic illustration of the formation mechanism of vaterite particles with
35 different morphologies.
36
37
38
39
40
41
42
43
44
45
46
47
48
49
50
51
52
53
54
55
56
57
58
59
60
61
62
63
64
65

Table 1 Morphology of the precipitates prepared by various conditions

Current / A	Temperature control	Morphology				
		Spherical	Rhombohedral	Hexagonal	Flower-like	Rod-like
0.2	No	Yes	Yes	No	Yes	No
0.4	No	Yes	Yes	No	Yes	Yes
0.4	Ice cooling	Yes	No	Yes	No	Yes
0.6	No	No	No	No	Yes	Yes

Figure1

[Click here to download high resolution image](#)

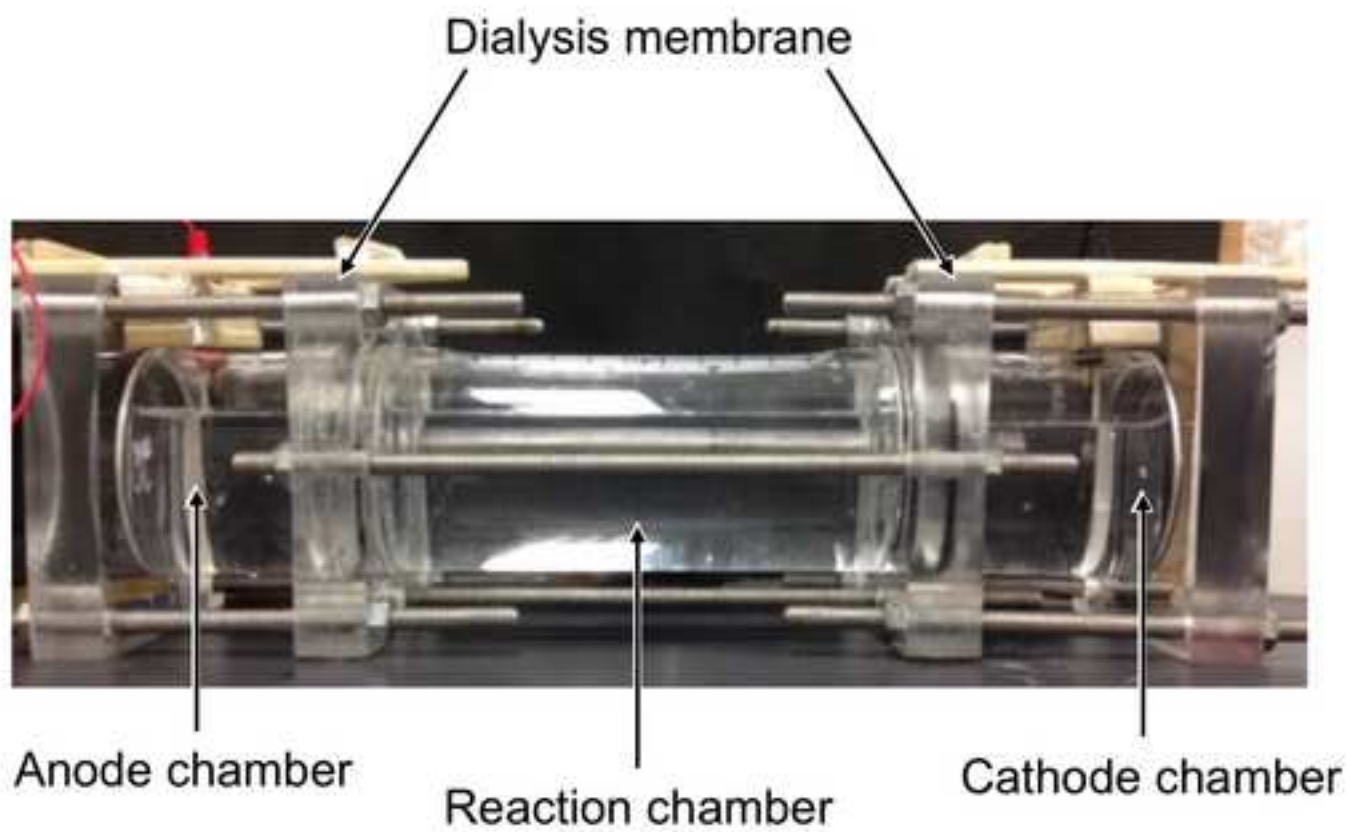


Fig. 1

Figure2

[Click here to download high resolution image](#)

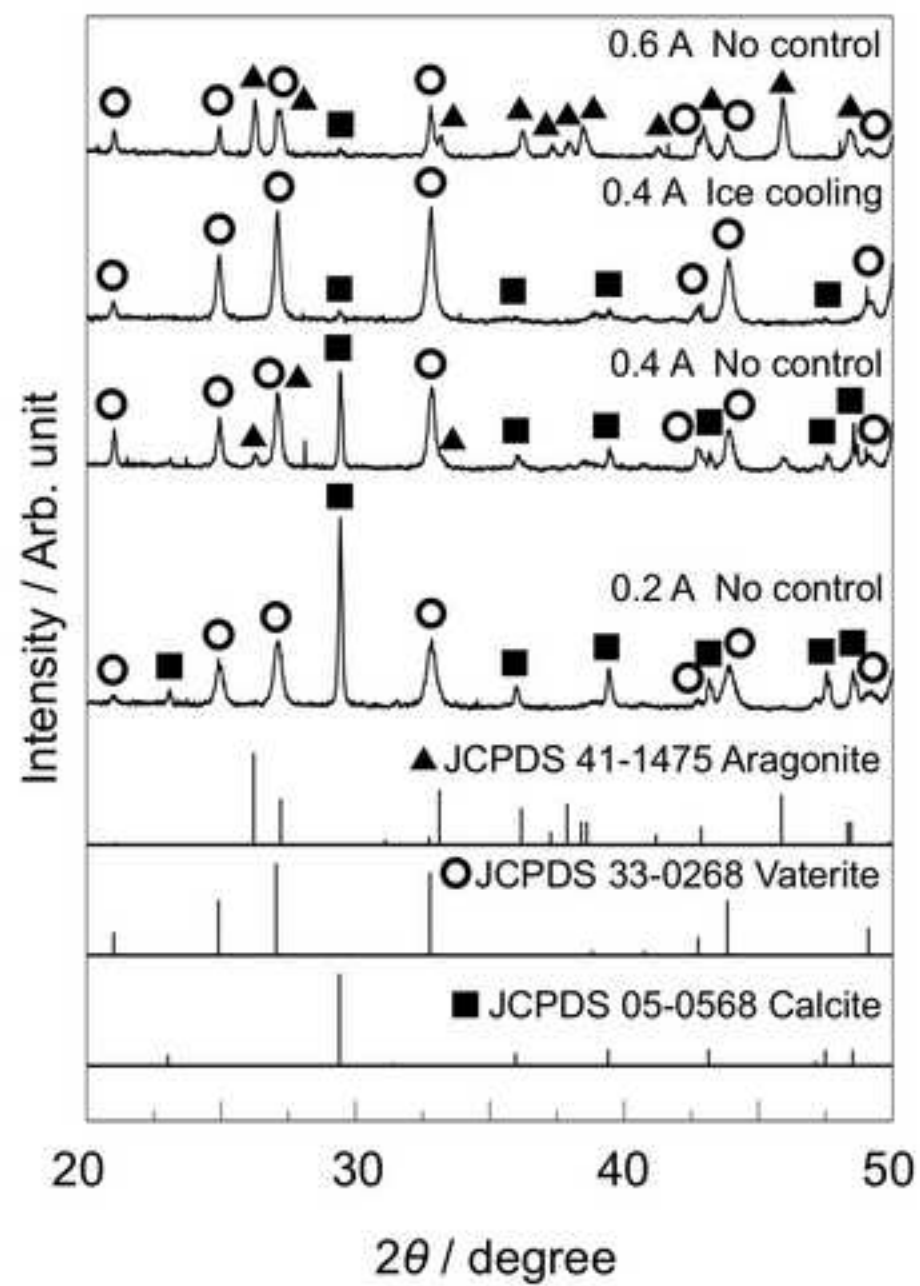


Fig. 2

Figure3

[Click here to download high resolution image](#)

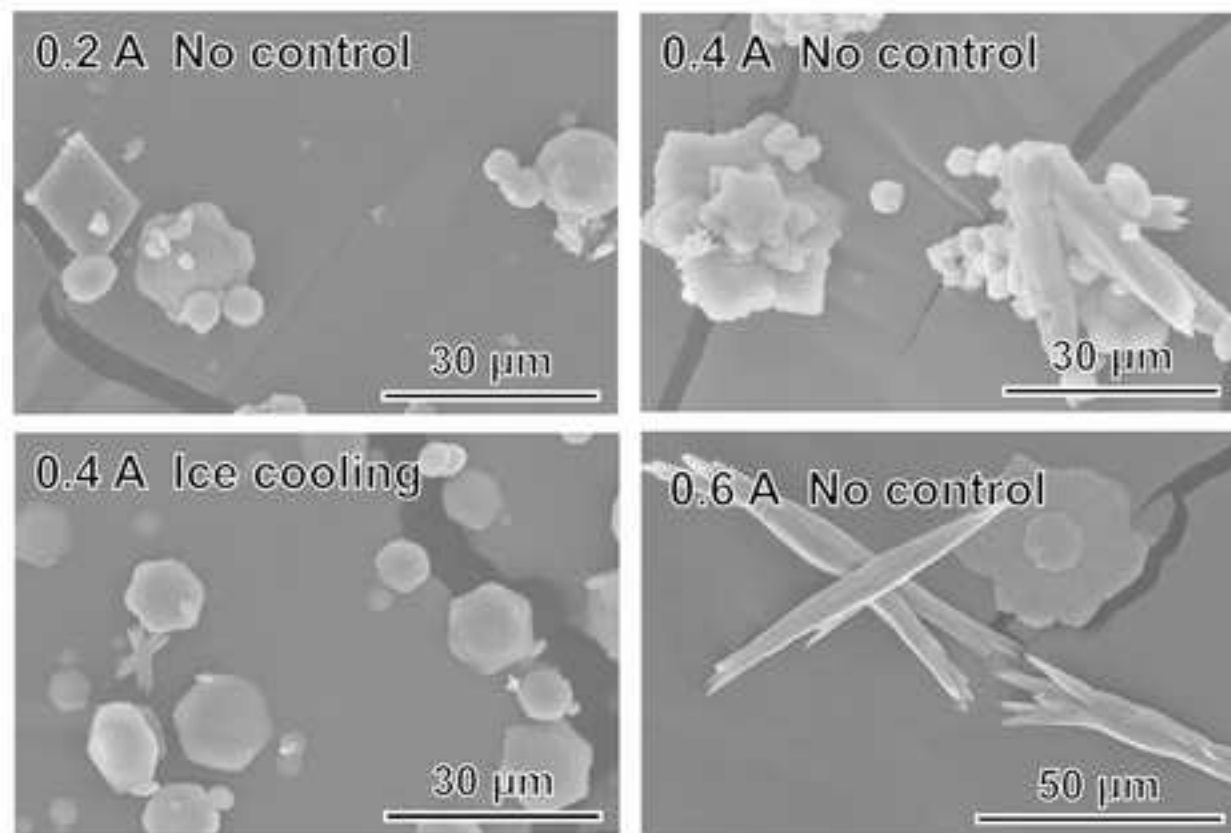
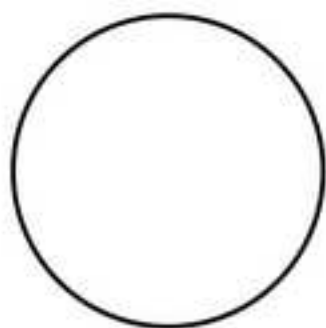


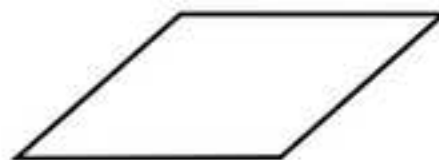
Fig. 3

Figure4

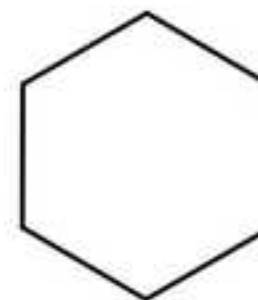
[Click here to download high resolution image](#)



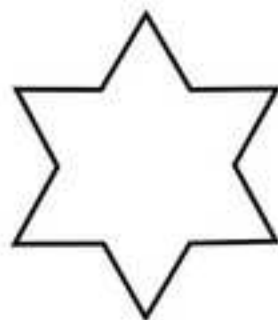
Spherical



Rhombohedral



Hexagonal



Flower-like



Rod-like

Fig. 4

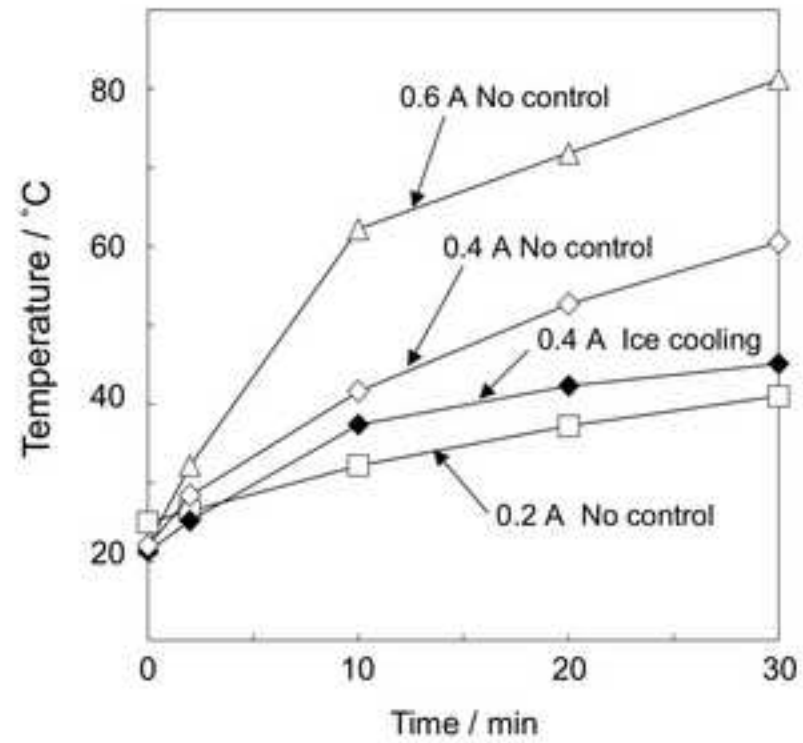


Fig. 5

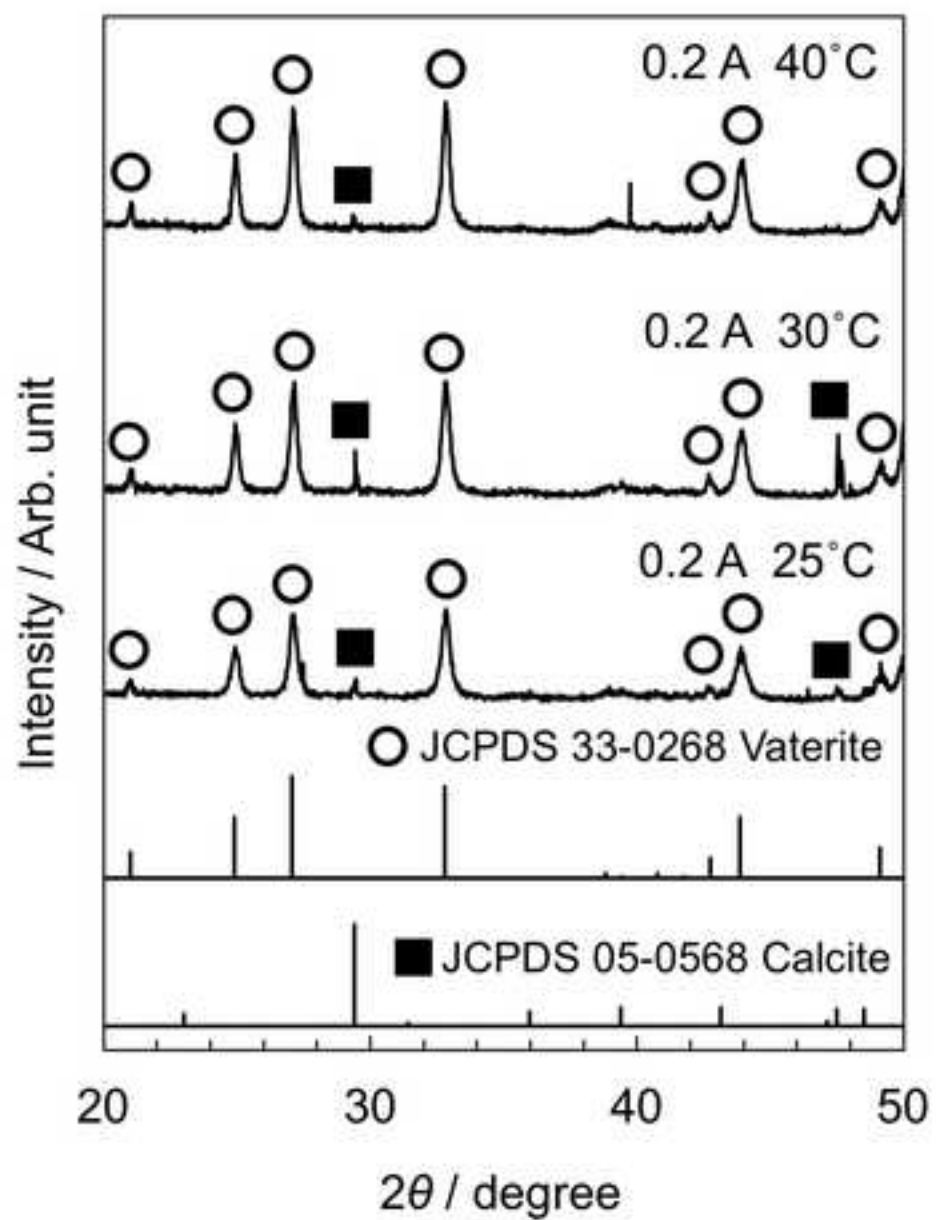


Fig. 6

Figure7

[Click here to download high resolution image](#)

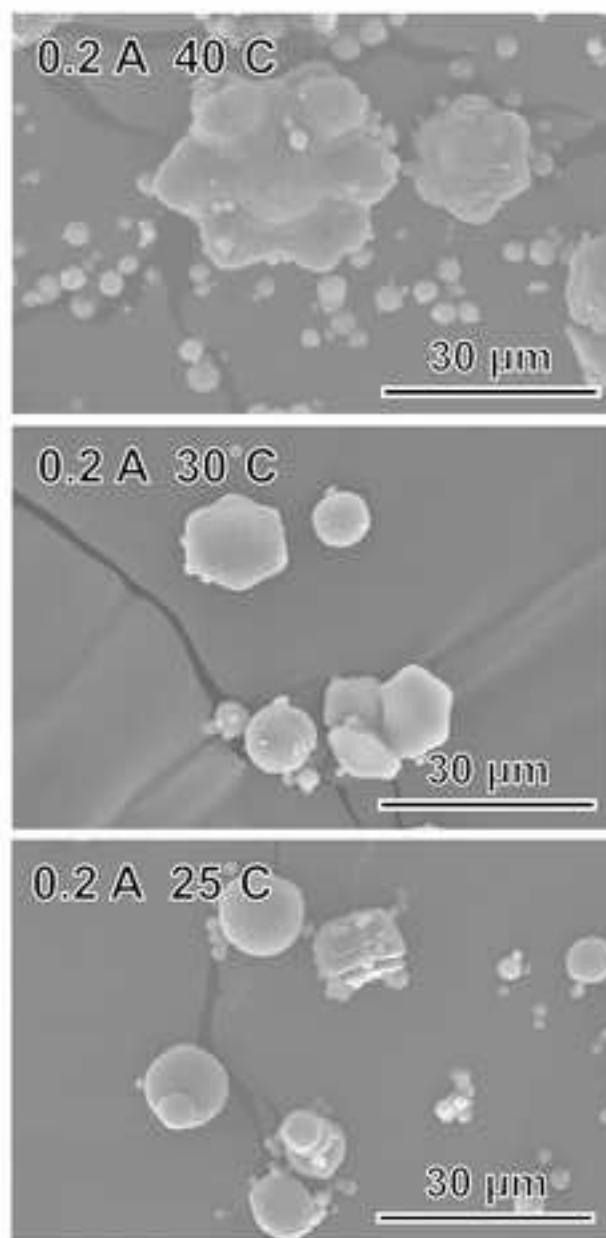


Fig. 7

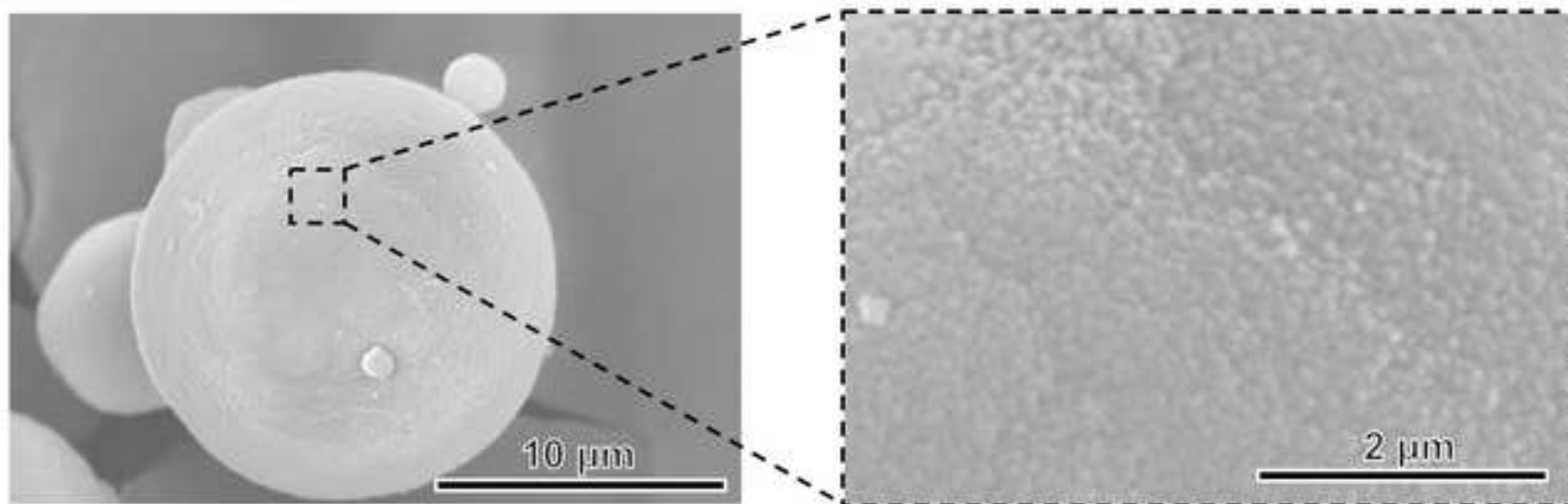


Fig. 8

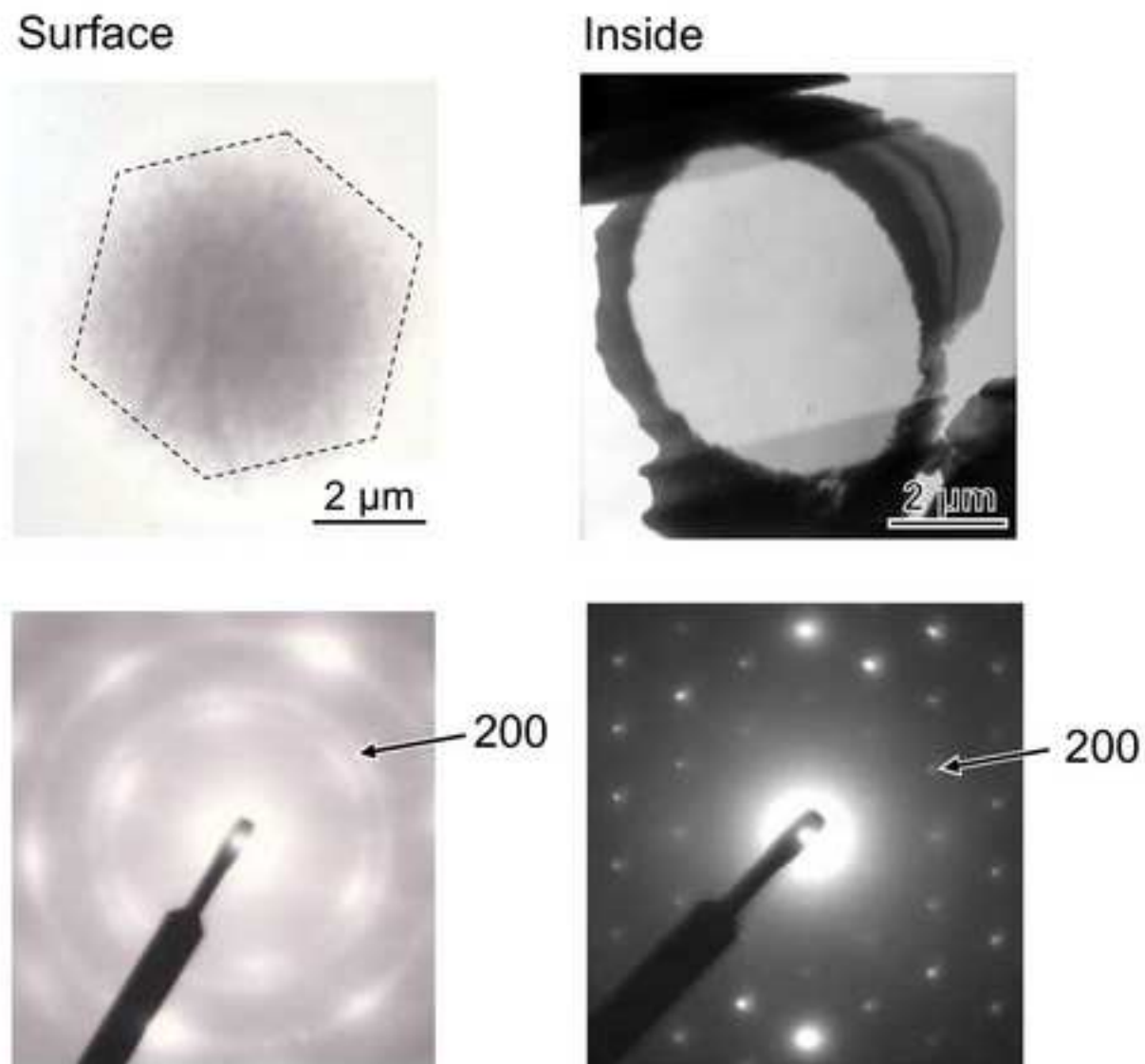


Fig. 9

Figure10

[Click here to download high resolution image](#)

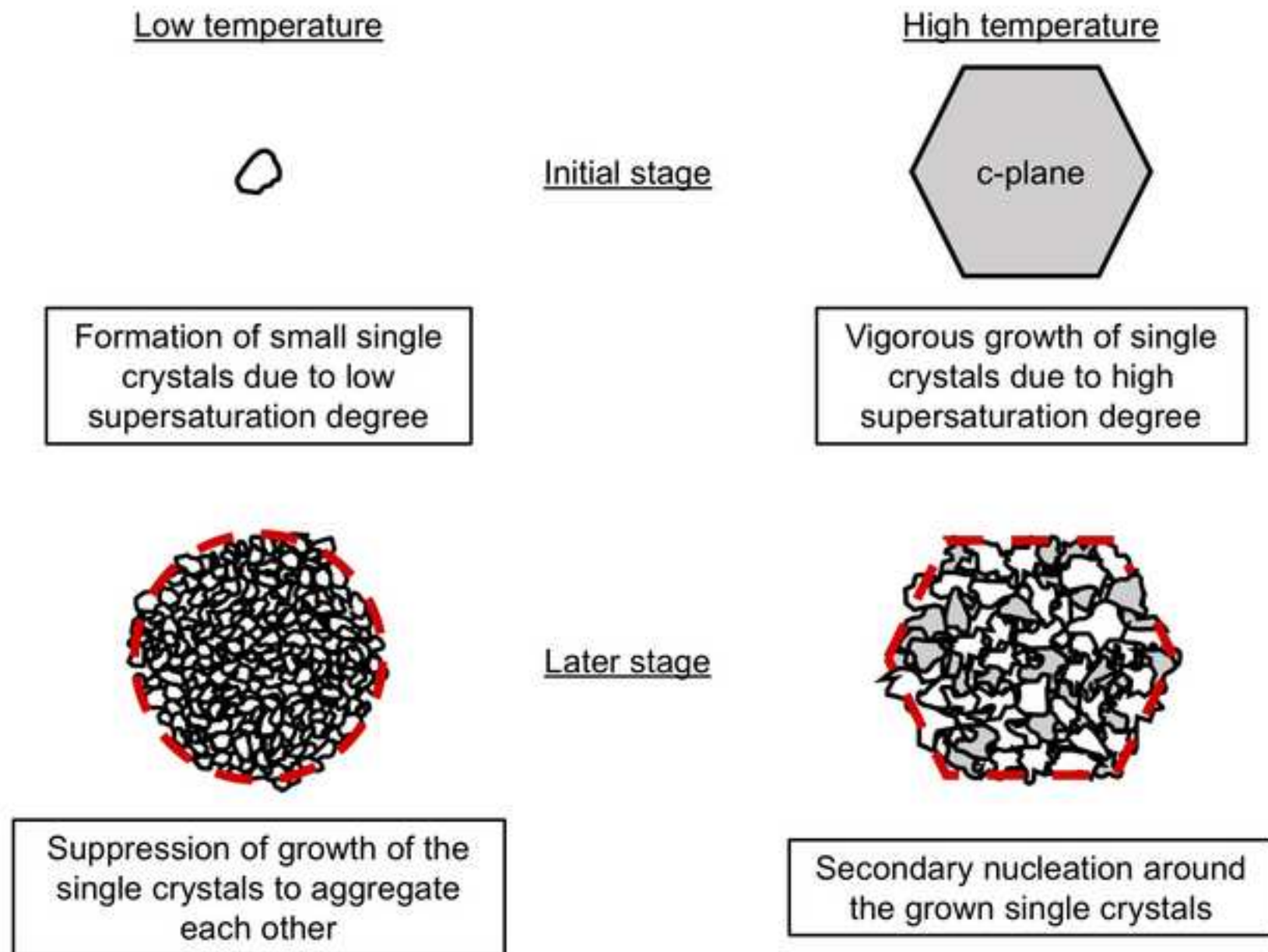


Fig. 10